Quantum mechanical study of the D+H2→HD+H reaction

N. AbuSalbi, D. J. Kouri, Y. Shima, and Michael Baer

Citation: The Journal of Chemical Physics **82**, 2650 (1985); doi: 10.1063/1.448261
View online: http://dx.doi.org/10.1063/1.448261
View Table of Contents: http://scitation.aip.org/content/aip/journal/jcp/82/6?ver=pdfcov
Published by the AIP Publishing

Quantum mechanical study of the $D+H_2 \rightarrow HD+H$ reaction

N. AbuSalbi[a)]
Department of Chemistry, University of Houston, Houston, Texas 77004

D. J. Kouri[a)]
Department of Chemistry and Department of Physics, University of Houston, Houston, Texas 77004

Y. Shima and M. Baer
Applied Mathematics, Soreq Nuclear Research Center, Yavne 70600, Israel

(Received 28 March 1984; accepted 20 September 1984)

A quantum mechanical study is made of the $D + H_2(v_i = 0,1) \rightarrow HD(v_f = 0,1,2) + H$ reactions within the infinite order sudden approximation (IOSA) for the total energy interval $0.28 \leq E_t \leq 1.28$ eV. Results at various stages of the calculation are given ranging from most detailed reactive transition probabilities through opacity functions and γ-dependent cross sections to total and state-to-state integral and differential cross sections, as well as rate constants. The cross sections and rate constants are compared with other available theoretical results and experiments. It is found that the IOSA total cross sections for $v_i = 0,1$ overlap very nicely with the corresponding quasiclassical trajectory cross sections, except for the tunneling region. A less satisfactory fit is obtained with the distorted wave born approximation results. The calculated rate constants are compared with experiment and a rather good fit is obtained, in particular for rate constants from the ground state.

I. INTRODUCTION

The quantum mechanical treatment of a three-dimensional atom–diatom reactive system is one of the main subjects of theoretical chemistry.[1] About a decade ago, when the first numerical results for $H + H_2$ reactions appeared in print, it seemed that the problem was solved.[2] However, difficulties associated with numerical instabilities and with the bifurcation into two nonsymmetric product channels slowed down the progress with this kind of treatment. This situation caused a change in the order of priorities. Whereas previously three to five groups were working on developing algorithms for yielding an exact solution and only one or two were considering approximate methods, now five to seven groups are developing approximations and only two or three groups are still working on the exact treatment.

Of the various approximations, the quasiclassical trajectory method (QCT) is fully developed and doing the calculations within this approach is simple.[3] The method is widely used and the results in many systems seem to be good. This seems to be the case for total integral cross sections when the energy is above threshold and for rotational state-to-state cross sections. The method is believed to be inadequate for vibrational state-to-state cross sections[4,5] and low temperature rate constants.[6] With regard to differential cross sections the situation is not clear.[6,7]

The other widely used method is the Distorted Wave Born Approximation (DWBA),[8] which is basically a first order quantum mechanical perturbation theory and therefore is expected to be accurate only when transition probabilities are small, namely around threshold. From the various applications it is difficult to estimate how good the results really are. It seems to produce reasonable relative results, such as rotational distributions,[8(e)] but is inaccurate for absolute cross sections.

Two other methods are variants of transition state theory. The canonical variational theory, the Marcus Coltrin Path Vibrational Adiabatic Ground State (CVT/MCPVAG) method[9] is the name of a three dimensional transition state version based, for the tunneling energy region, on the Marcus Coltrin path[10] which is basically a "corner cutting" path. The model applies to three-dimensional systems because the motion is performed on the quantized energy as obtained from all bound degrees of freedom (i.e., vibration and bend). The method is found to produce quite good rate constants in the low temperature region.[9] The Adiabatic Infinite Order Sudden Approximation (AD-IOSA)[11] is another three-dimensional transition state model. Here the transition state theory is applied for every bend angle $\gamma = \cos^{-1}(\hat{R} \cdot \hat{r})$ and the final cross section follows from the integration over γ. In a sense the model is close to the ordinary reactive IOSA. The model was applied mainly to systems with dynamic barriers located at the entrance channel and for these very encouraging results were obtained.

A new model, recently introduced, is the Bending Corrected Rotating Linear Model (BCRLM).[12] This model is basically a collinear system modified in the following way: (a) the dynamics is performed on a bend eigenstate (instead of the bend angle $\gamma = 0$) and in this sense it is

[a)] Supported under R. A. Welch Foundation Grant E-608.

 0021-9606/85/072650-12$02.10

related to the CVT/MCPVAG model;[9] (b) the potential also includes an (orbital) centrifugal potential energy term which not only has an effect on the dynamics, but also effects the asymptotic boundary conditions.[13] The BCRLM method is designed to treat systems for which the bend is adiabatic and this is most likely to be relevant in the threshold region.

In this paper we present results calculated within the framework of the IOSA.[13-19] The IOSA is based on quasicollinear S-matrix elements derived by solving γ-dependent collinear-type Schrödinger equations.[13] The IOSA has been found to yield total cross sections which, except for the low energy region, fit very nicely both exact quantum mechanical (H_2 + H)[14] and coupled states[20] [F + H_2, ^{15}H(D) + HCl, ^{17}H(D) + HBr[18]] results, as well as QCT results [F + $H_2(D_2)$[7,21]]. Regarding more detailed information, such as vibrational state-to-state differential and integral cross sections, generally satisfactory agreement is obtained between IOSA and coupled states (CS) results for D(H) + HCl[17] and D(H) + HBr[18] systems, as well as for F + H_2,[15,20] but agreement with similar QCT results[7,21] [F + $H_2(D_2)$[15,16]] is rather poor.

This paper deals with the D + H_2 (v_i = 0, 1) → HD (v_f = 0, 1, 2) + H reactions.[19] The calculations are done employing the Siegbahn–Liu–Truhlar–Horowitz (SLTH) surface[22] which is an *ab initio* surface, considered to be the most accurate to date.

In the next section two types of results are given: primitive results, such as γ, l (orbital quantum number) and E_t (total energy) dependent probabilities, for gaining insight and more physical results, i.e., integral and differential, state-to-state and total cross sections and rate constants. These are then compared with results obtained from the previously mentioned methods and with experiment.[23-26] The discussion and a summary are given in the last section.

II. RESULTS

The results discussed here are to two types: primitive results, such as l and γ dependent probabilities which are of interest for developing other approximations and for interpreting results and the results of more physical content, such as integral and differential cross sections and rate constants.

A. Primitive results—γ_λ and l dependent probabilities

In Figs. 1–3 the reactive probabilities $P(l, \gamma_\lambda, E_t, v_i, v_f)$ as a function of l for different values of γ_λ, E_t, v_i, and v_f are shown. In Fig. 1 are presented the (v_i = 0 → v_f = 0) transition probabilities for four different energies. The position of the peak can be seen to depend on both γ_λ and E_t, shifting to higher l values as either E_t increases or γ decreases. It is also notable that the functions increase, as a function of l, at a slow rate. It seems that a more symmetric shape would be obtained by plotting the probability functions as a function of l^2 [or $l(l+1)$], which is the coefficient of the repulsive centrifugal term in the entrance channel.

The (v_i = 1 → v_f = 1) transition probabilities for the two higher energies are shown in Fig. 2. In general, the shape of the curves is the same as in the previous case, but the range of l values is shorter due to the lower initial translational energy; for the two energies E_t = 1.086 and 1.266 eV the corresponding translational energies are E_{tr} = 0.30 and 0.48 eV as compared with E_{tr} = 0.816 and 0.946 eV in the previous case.

Figure 3 is made up of three parts each showing four curves related to three vibrational transitions. All the curves are for E_t = 1.266 eV but each part is for a different γ_λ. Here the aim is to show, in a direct way, the source of possible differences between the corresponding

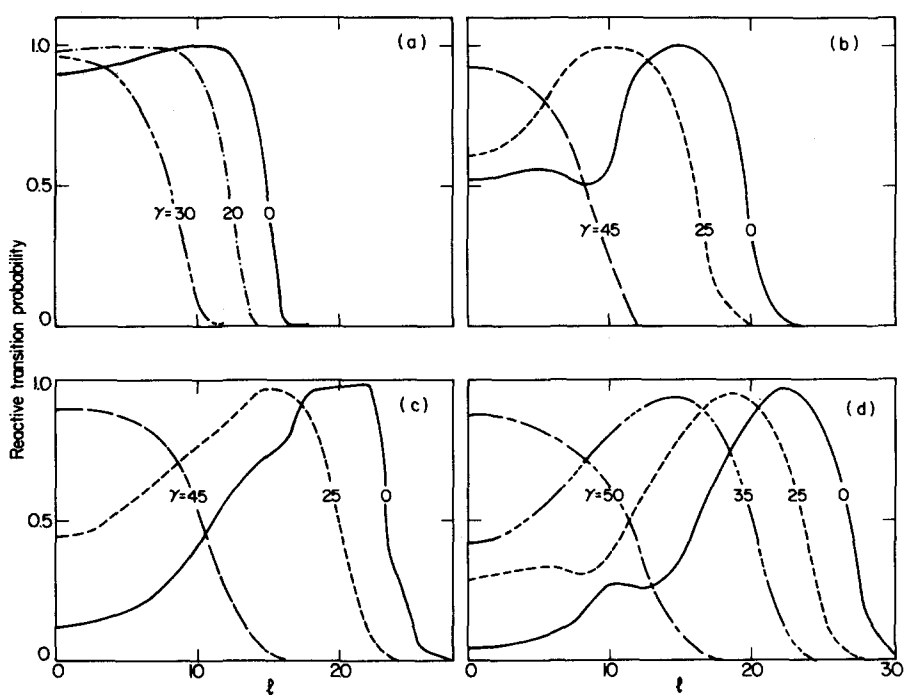

FIG. 1. Primitive reactive v_i = 0 → v_f = 0 transition probabilities as a function of l for various γ_λ angles. (a) E_{tot} = 0.7503 eV; (b) E_{tot} = 0.9203 eV; (c) E_{tot} = 1.0865 eV; (d) E_{tot} = 1.2665 eV.

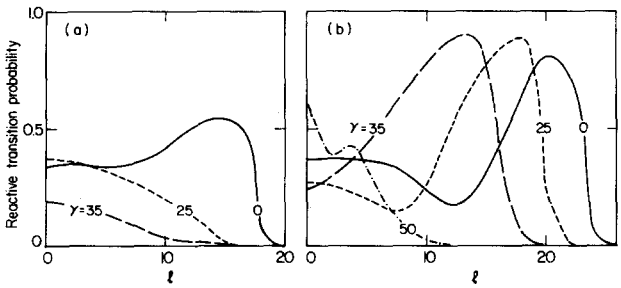

FIG. 2. Primitive reactive $v_i = 1 \rightarrow v_f = 1$ transition probabilities as a function of l for various γ_λ angles. (a) E_{tot} = 1.0865 eV; (b) E_{tot} = 1.2665 eV.

integral cross sections. For instance, it is evident that the (1 → 1) and the (0 → 0) transition curves overlap very nicely at the low l values, but the (1 → 1) curves reach their peak values at lower l values and then decrease to zero at a faster rate due to the lack of translational energy which is needed to surmount the centrifugal barrier. On the other hand, two nonadiabatic transition probability curves (1 → 0) and (0 → 1) are, in general, close to each other for most l values, but in particular they overlap very nicely at the higher l values.

The reactive probabilities $P(l, \gamma_\lambda, E_t, v_i, v_f)$ as a function of l for different values of γ_λ, E_t, v_i, and v_f are shown in Figs. 4–6. In Fig. 4, which gives the 0 → 0 transition probabilities for E_t = 0.75 eV, it is seen that even for such a low energy (E_{tr} = 0.48 eV) the γ_λ region extends to γ_λ = 45°, although it shrinks rapidly as l increases. In general the maximum is reached for γ_λ = 0. The adiabatic probabilities, i.e., 0 → 0 and 1 → 1 curves, for the energy E_t = 1.086 eV are presented in Fig. 5. Due to an increase in energy not only the l and γ_λ regions increase, but also the peaks of the various probability curves start to move away from the γ_λ = 0 value (the collinear arrangement) to higher γ_λ values. Thus, for instance, for l = 0 the largest reactive transition probabilities are obtained around γ_λ = 45°. These kinds of features are even more enhanced for E_t = 1.266 eV as can be seen from Fig. 6. The γ_λ range is now approaching the value of γ_λ = 70°, a larger number of l's is contributing to the reaction and the peaks of the various curves keep moving towards higher γ_λ values. Nevertheless, the adiabatic transition probabilities 0 → 0 and 1 → 1 are much larger than the nonadiabatic probabilities 0 → 1 and 1 → 0.

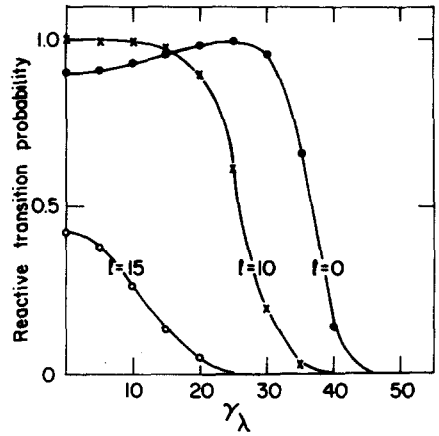

FIG. 4. Primitive reaction $v_i = 0 \rightarrow v_f = 0$ transition probabilities as a function of γ_λ for different l values and for E_{tot} = 0.7503 eV.

In Fig. 7 the reactive probabilities $P(l, \gamma_\lambda, E_t, v_i; \Sigma v_f)$ are presented as a function of l for three different γ_λ values, two values of v_i and two energies, i.e., E_t = 0.75 and 1.266 eV. The results allow one to gain insight into the importance of the distribution of the energy between the two modes of motion for promoting the reaction. Results with the same translational energy, i.e., E_{tr} = 0.48 eV and results with same total energy, i.e., E_t = 1.266 eV are compared. Curves (1) and (2) are for v_i = 0 and 1, respectively, but derived for the same translational energy. Curves (2) and (3) are with v_i = 1, 0, respectively, but with the same total energy (consequently the translational energy for v_i = 0 is much higher). The main point to be noticed is that total energy, as compared with translational energy, is more crucial for having a reaction, however, for a given total energy, the translational mode is more important in promoting the reaction.

As a last set of primitive results we show reactive transition probabilities as a function of energy for different values of γ_λ and l. In Figs. 8(a)–8(c) the results for the 0 → 0 transition are shown and in Figs. 8(d) and 8(e) the results for 1 → 1 transitions are given. In each figure there are two or three curves which correspond to different l values. The figures show very clearly how the threshold

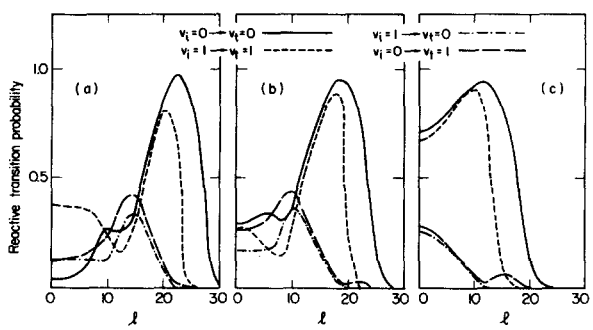

FIG. 3. Primitive reactive state-to-state transition probabilities as a function of l for E_{tot} = 1.2665 eV. (a) γ_λ = 0°; (b) γ_λ = 25°; (c) γ_λ = 40°.

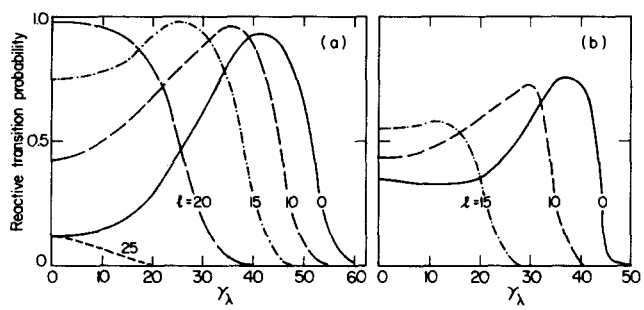

FIG. 5. Primitive reactive adiabatic transition probabilities as a function of γ_λ for different l values and for E_{tot} = 1.0865 (a) $v_i = 0 \rightarrow v_f = 0$; (b) $v_i = 1 \rightarrow v_f = 1$.

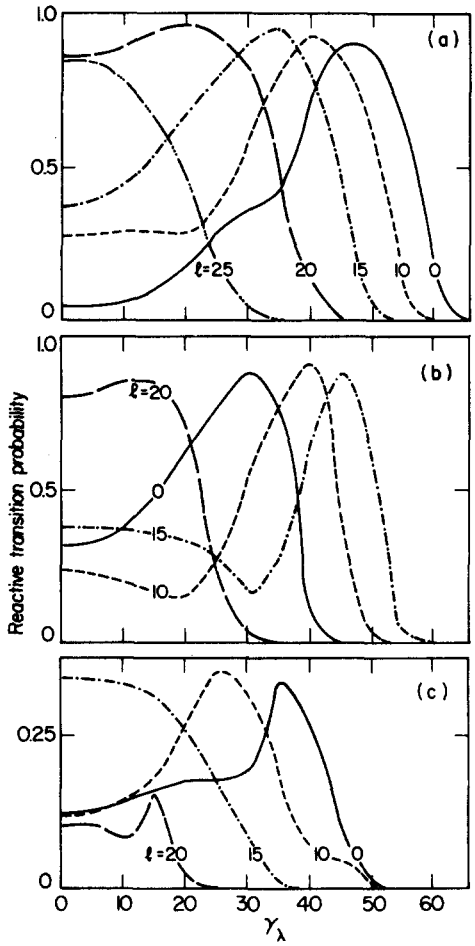

FIG. 6. Primitive reactive transition probabilities as a function of γ_λ for different l values and for E_{tot} = 1.2665 eV. (a) $v_i = 0 \rightarrow v_f = 0$; (b) $v_i = 1 \rightarrow v_f = 1$; (c) $v_i = 1 \rightarrow v_f = 0$.

region is affected by varying either l or γ_λ. All the curves seem to be simply shifted to higher energies as either l or γ_λ is increased.

B. Angle averaged results

In Figs. 9 and 10 the angle average probabilities (or opacity functions) $P(l, v_i, v_f)$ are presented. These are defined as

$$P(l, E_t|v_i, v_f) = \tfrac{1}{2}\int_{-1}^{+1} d(\cos\gamma_\lambda) P(l, \gamma_\lambda, E_t|v_i, v_f). \quad (1)$$

The results for different energies and different initial and final states are given in Fig. 9. In general, all the curves are of similar shape with a maximum at $l = 0$ and then decreasing monotonically to zero with increasing l. The adiabatic reactions, i.e., $(0 \rightarrow 0)$ and $(1 \rightarrow 1)$ are, for a given l, seen to be more probable and also to extend to larger l values than the nonadiabatic ones. Of the nonadiabatic processes the reactions with $v_i = 0$ are more efficient indicating translation is more efficient in promoting a reaction than vibration.

In Fig. 10 the opacities for three different cases are presented. Curves (1) and (2) are for results with identical translational energy, i.e., E_{tr} = 0.48 eV, whereas curves (2) and (3) are for results with identical total energies E_t = 1.266 eV. Curves (1) and (3) are for $v_i = 0$ and curve (2) for $v_i = 1$. As in Fig. 7 these curves are presented to show (a) that total energy is more important than translational energy in promoting a reaction; (b) that in the case where the total energy is the same, the translational mode is more efficient than the vibrational one in causing the system to react.

C. *l*-summed results: γ-dependent cross sections

γ_λ-dependent total and vibrational state-to-state cross sections are defined as

$$\sigma(\gamma_\lambda|E_t, v_i, v_f) = \frac{\pi}{k_{v_i}^2}\sum_l (2l+1)P(l, \gamma_\lambda, E_t|v_i, v_f) \quad (2)$$

and shown in Figs. 11 and 12. The vibrational (γ-dependent) cross section for E_t = 1.266 eV is given in Fig. 11. The results with $v_i = 0$ are seen to be lower than those with $v_i = 1$, but extend to larger γ_λ values. The curves themselves are monotonic decreasing functions.

The partial total cross sections defined as

$$\sigma(\gamma_\lambda|E_t, v_i) = \sum_{v_f} \sigma(\gamma_\lambda|E_t, v_i, v_f) \quad (3)$$

are presented in Fig. 12 for three energies. The relative increase of $\sigma(\gamma|E_t, v_i = 1)$ with respect to $\sigma(\gamma|E_t, v_i = 0)$ as a function of E_t is evident. For the lowest energy $\sigma(\gamma|E_t, v_i = 0) > \sigma(\gamma|E_t, v_i = 1)$ along the whole γ_λ range; however, as E_t increases, this is no longer true. Here, the higher E_t is, the larger is the range of γ_λ values for which $\sigma(\gamma|E_t, v_i = 1) > \sigma(\gamma|E_t, v_i = 0)$.

D. Differential cross sections

Total and state-to-state l-average reactive differential cross sections (degeneracy averaged over m_λ and summed over m_v and j_v) are presented in Figs. 13 and 14. The total differential cross sections for the energies E_t = 0.7503, 0.9202, 1.0865, and 1.2665 eV are shown in Fig. 13. The present results are compared [Fig. 13(a)] with the corresponding results from a QCT calculation

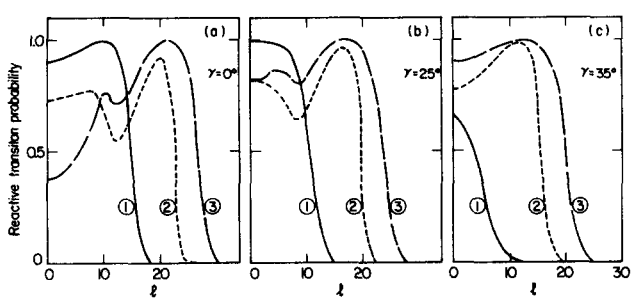

FIG. 7. Total primitive reactive transition probabilities as a function of l for different γ_λ angles. Curves (1): $v_i = 0$; E_{trans} = 0.48 eV; curves (2): $v_i = 1$; E_{trans} = 0.48 eV and for $v_i = 1$; E_{tot} = 1.2665 eV; curves (3): $v_i = 0$; E_{tot} = 1.2665 eV.

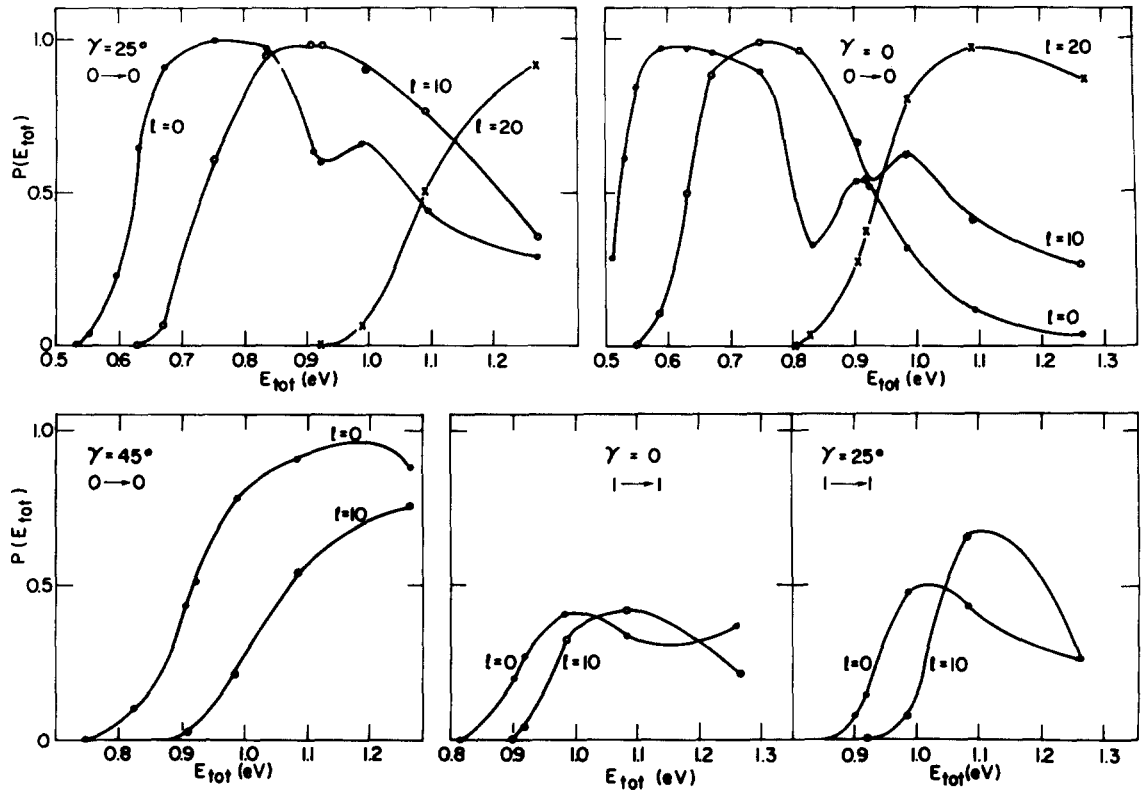

FIG. 8. Primitive reactive state-to-state probabilities as a function of total energy.

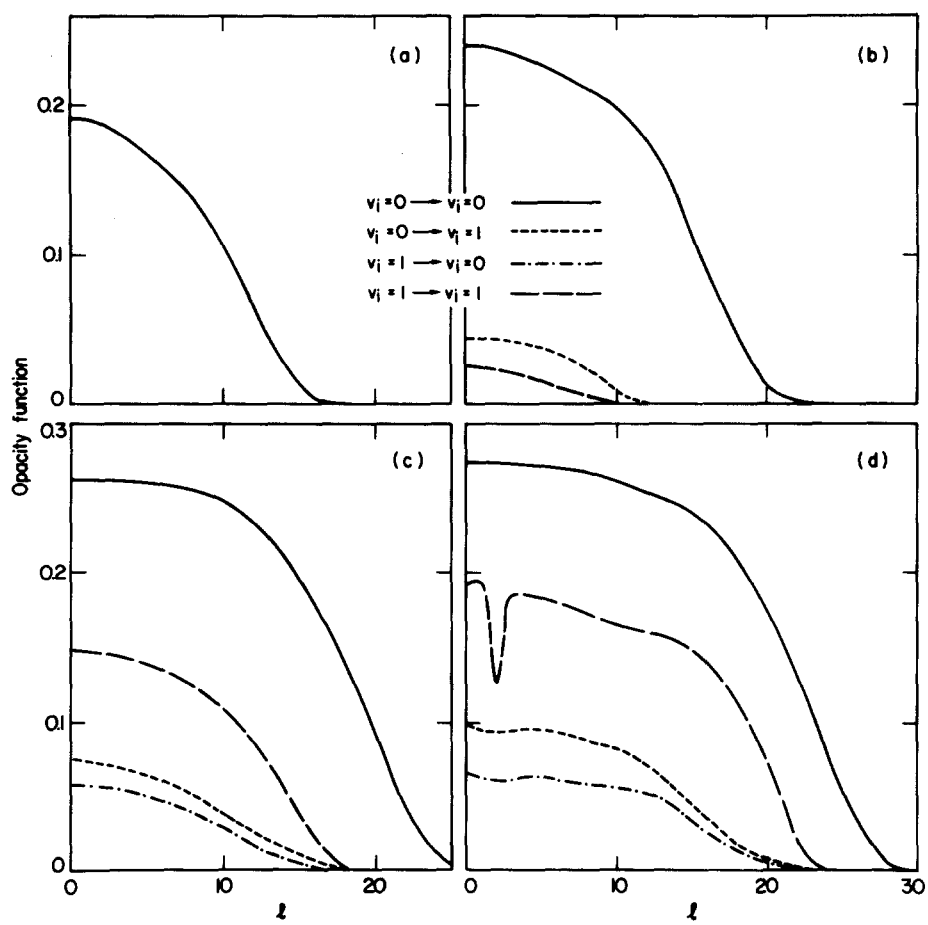

FIG. 9. State-to-state opacity functions [see Eq. (1)] for different energies. (a) E_{tot} = 0.7503 eV; (b) E_{tot} = 0.9203 eV; (c) E_{tot} = 1.0865 eV; (d) E_{tot} = 1.2665 eV.

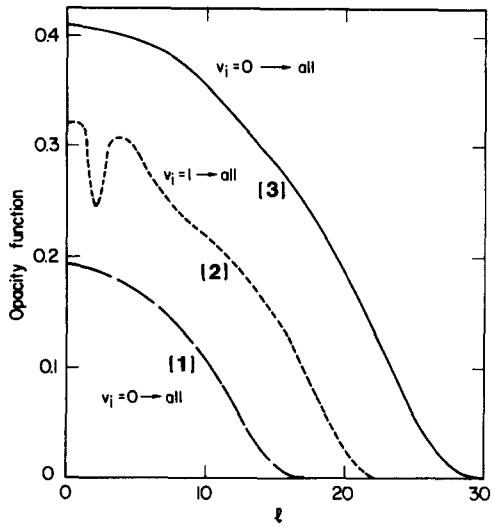

FIG. 10. Total opacity functions [see Eq. (1)]: (1) $v_i = 0 \rightarrow$ all, E_{tot} = 0.7503 eV; (2) $v_i = 1 \rightarrow$ all, E_{tot} = 1.2665 eV; (3) $v_i = 0 \rightarrow$ all, E_{tot} = 1.2665 eV. The two curves $v_i = 0$ (E_{tot} = 0.7503 eV) and $v_i = 1$ (E_{tot} = 1.2665 eV) are at the same translational energy, i.e., E_{trans} = 0.48 eV.

and a DWBA calculation, all obtained employing the same potential energy surface. All three curves are seen to be backward peaking, but the IOSA curve is broader than the two others. In each of the other figures, [13(b)–13(d)] two curves are shown; one for $v_i = 0$ and the other for $v_i = 1$. At the lower energy the $v_i = 0$ curve is much broader, but as the energy increases the $v_i = 1$ curve begins to swell, whereas the $v_i = 0$ curve hardly changes so that for the highest energy the $v_i = 1$ distribution is now broader. Another feature is the sidewards shift of the $v_i = 0$ curve as the energy increases. This tendency is less apparent for $v_i = 1$.

In Fig. 14 state-to-state differential cross sections are presented. In each box there are three or four curves, one for each energy. In all cases the curves are broader and the peaks are more shifted sidewards, the higher the energy. Another feature is that the adiabatic state-to-state distributions are always broader than the nonadiabatic ones. For a general reaction involving both attractions and repulsions, there is no simple direct relation between the range of l values that contribute to the reactive transition and the detailed angular distribution of the products. However, to a first approximation, the lower l values tend to scatter at larger angles than the higher l values when the interaction is repulsive. In this purely repulsive case, advantage can be taken of the fact that

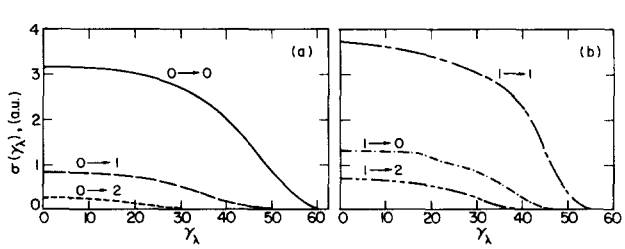

FIG. 11. State-to-state γ-dependent cross sections [see Eq. (2)] for E_{tot} = 1.2665 eV. (a) $v_i = 0$; (b) $v_i = 1$.

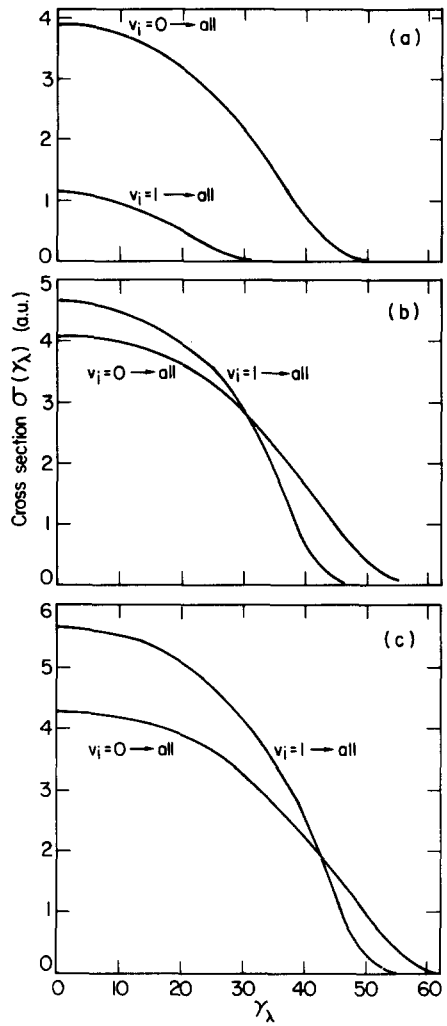

FIG. 12. Total γ-dependent cross sections [see Eq. (2)]. (a) E_{tot} = 0.9203 eV; (b) E_{tot} = 1.0865 eV; (c) E_{tot} = 1.2665 eV.

the value of l corresponds approximately to the classical impact parameter b, so that the low l values are related to more "head-on" collisions. These sample the short range repulsions more strongly and therefore tend to yield large angle scattering. The larger l values correspond approximately to larger b values or more grazing collisions. Reaction for such collisions results more from striping out an H atom as the projectile flies by the target H_2 and should yield more forward scattering. Thus, we expect a shift from large angle to smaller angle scattering to occur as the range of l values contributing significantly increases. We have already noted also that as the energy increases, more l values contribute to the reactive process and the dominant contributions are usually from the higher l values (see Figs. 1–9). As a consequence, the angular distribution becomes broader and the peak of the distribution moves towards smaller angles as the energy increases. This effect was encountered in previous studies of the F + $H_2(D_2)$ systems[15,16] and is the case here also. From Figs. 3 and 9 it can be seen that the adiabatic reactive transitions extend to larger l values than the nonadiabatic ones. This may be a consequence of the necessity of the collision to sample the hard short range

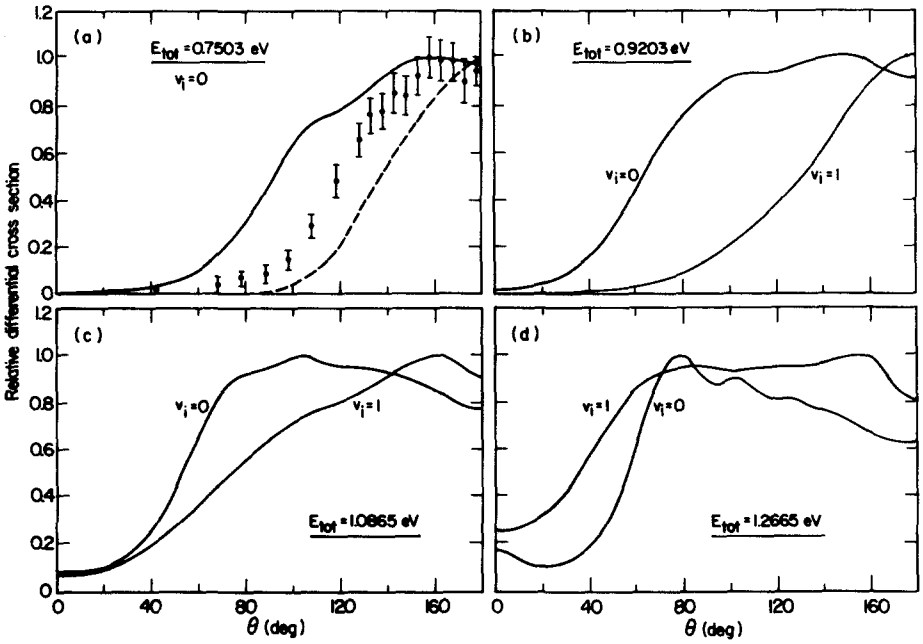

FIG. 13. Total differential cross sections for different energies. (a) E_{tot} = 0.7503 eV, — present IOSA results; --- DWBA results [ref. 8(d)]; ♦ QCT results (Ref. 27); (b) E_{tot} = 0.9203 eV; (c) E_{tot} = 1.0865 eV; (d) E_{tot} = 1.2665 eV.

repulsions of the potential surface in order to transfer energy between translation and vibrational motion. Since only the lower l values permit the particles to approach so closely to one another, one would expect the nonadiabatic reaction to occur for lower l values than the adiabatic reaction. This is probably the reason why the adiabatic angular distributions extend to lower angles than the nonadiabatic ones. The situation is different when comparison is made with respect to the *total* reactive transitions from $v_i = 0$, as compared with those from $v_i = 1$. In all cases the reactive process from $v_i = 0$ extends to larger l values than from $v_i = 1$. This is probably the consequence of the higher translational energy for $v_i = 0$ total cross sections compared to $v_i = 1$ at the same total energy. As a result, higher l values contribute to the $v_i = 0$ total cross sections. This can be seen in Figs. 3 and 5–10. From Figs. 13(b) and 13(c) it is seen that the angular distribution for $v_i = 0$ is broader than the $v_i = 1$ distribution, as expected. However, a different situation is encountered in Fig. 13(d), where $v_i = 1$ becomes broader although it is obtained from a shorter l range (see Fig. 10). Still the peak of the $v_i = 0$ distribution is located at a much lower angle which, according to previous experience, is also due to contributions of higher l values.

E. Total and vibrational state-to-state cross sections

The total and vibrational state-to-state integral cross sections are given in Fig. 15 and Table I. In the table we

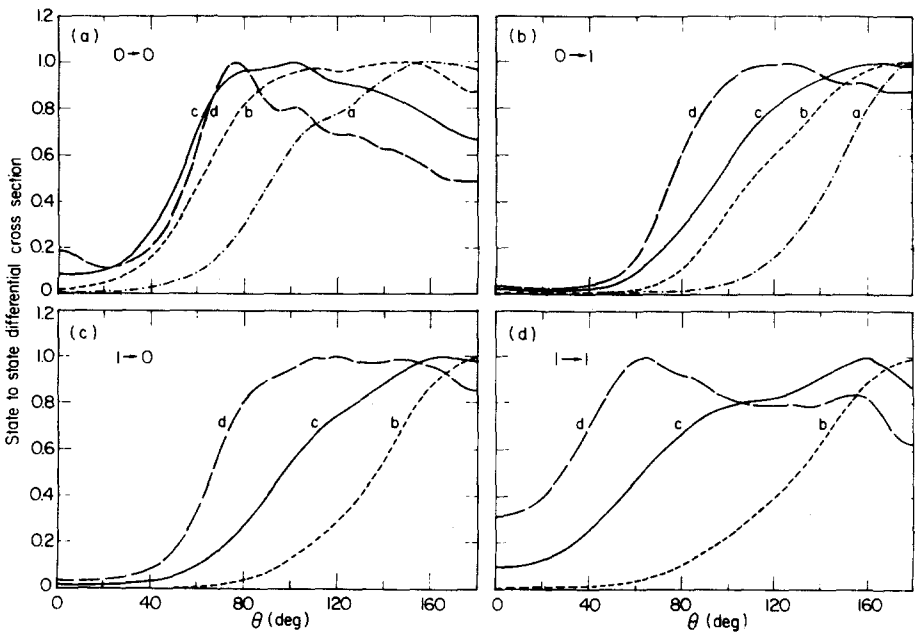

FIG. 14. State-to-state differential cross sections. Curve (a) is for E_{tot} = 0.7503 eV; curve (b) is for E_{tot} = 0.9203 eV; curve (c) is for E_{tot} = 1.0865; curve (d) is for E_{tot} = 1.2665 eV.

list only our IOSA results, but in Figs. 15(a)–15(c) the present results are compared with those obtained by various other methods.

In Fig. 15(a) four kinds of results for $v_i = 0$ are given; i.e., the l-in, l-av, QCT,[27] and DWBA[8(d),8(e)] results. The QCT results[27] follow the l-av curve very nicely, the l-in curve is consistently below the l-av curve (a fact noticed in all previous studies), and the DWBA curve is below the IOSA curve in the low energy range and then increases very rapidly as a function of E, so that it becomes much higher than the IOSA curves. In Fig. 15(b) four kinds of results for the total cross sections for $v_i = 1$ are given, namely, l in, l av, QCT,[27] and CL-AD-IOS.[11(b)] Again the lowest curve is the l-in curve. The QCT together with CL-AD-IOS[11(b)] results overlap the l-av curve very nicely at low energy, but then differences on the order of 10% to 20% are observed as the energy increases.

In Fig. 15(c) the integral vibrational state-to-state $v_i = 1 \rightarrow v_f = 0, 1$ cross sections are represented. Here the l-av IOSA results are compared with those due to the DWBA treatment.[8(d)] The DWBA cross sections are in most cases seen to be much larger, sometimes more than a factor of 4 than the IOSA cross sections.

The IOSA branching ratios, defined as

$$\lambda(E_t|1, 0) = \sigma(E_t|v_i = 1, v_f = 1)/\sigma(E_t|v_i = 1, v_f = 0) \quad (4)$$

are presented in Fig. 15(d) where the adiabatic process is seen to be about four times more favored than the nonadiabatic process. Another feature is the strong dependence of $\lambda(E_t|1, 0)$ on the energy. This fact is not necessarily an indication that the adiabatic process becomes more dominant as the energy increases. For instance, at $E_{\text{trans}} = 0.48$ eV the value of $\lambda(E_t|1, 0)$ is about 4, but since at this energy also the state $v_f = 2$ is open (see Table I), the measure for the adiabaticity is the ratio

$$\lambda_{\text{ad}} = \frac{\sigma(E_t|v_i = 1, v_f = 1)}{\sigma(E_t|v_i = 1, v_f = 0) + \sigma(E_t|v_i = 1, v_f = 2)} \quad (5)$$

and this value is only ~3.2.

F. Rate constants

The rate constants are shown in Fig. 16 and summarized in Tables II and III. The results for $v_i = 0$ are compared in Fig. 16(a) with the QCT and experimental results[23,24]; similar results for $v_i = 1$ are given in Fig. 16(b). The branching ratios for the rate constants are shown in Fig. 16(c). The QCT results follow the IOSA curves rather well [Figs. 16(a) and 16(b)] although they are always somewhat below them. This is, in particular, the case for $v_i = 1$. The comparisons with experimental results are also encouraging. For $v_i = 0$, the experimental results overlap the IOSA curves rather well, except for

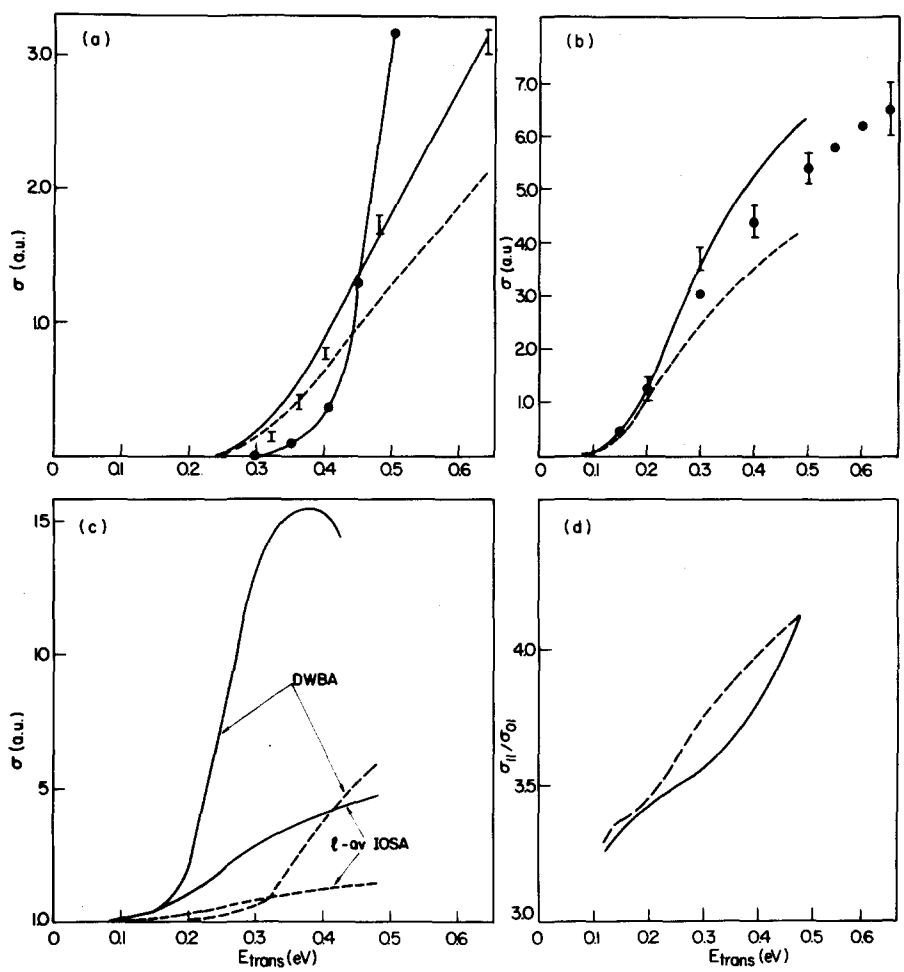

FIG. 15. Integral cross sections as a function of energy. (a) Total cross sections for $v_i = 0$. — l-av results; --- l-in results; ●—● DWBA results [refs. 8(d) and (e)]; I QCT results (Ref. 27); (b) total cross sections for $v_i = 1$. — l-av results; --- l-in results; ● CL ADIOSA results [Ref. 11(b)]; I QCT results (Ref. 27); (c) vibrational state-to-state cross sections. — $v_i = 1 \rightarrow v_f = 1$ (adiabatic transitions); --- $v_i = 1 \rightarrow v_f = 0$ (nonadiabatic transition); (d) IOSA vibrational branching ratio — l-av; --- l-in.

TABLE I. Integral vibrational state-to-state and total cross sections ($bohr^2$).

	$v_i = 0$					$v_i = 1$				
E_{tot}	E_{trans}	$\sigma_{0\to0}$	$\sigma_{0\to1}$	$\sigma_{0\to2}$	$\sigma_{0\,tot}$	E_{trans}	$\sigma_{1\to0}$	$\sigma_{1\to1}$	$\sigma_{1\to2}$	$\sigma_{1\to tot}$
0.5103	0.240	0.0135[a]	...	...	0.0135		...	...	...	...
		0.0124[b]	...	...	0.0124		...	...	...	...
0.5303	0.260	0.0374	...	...	0.0374		...	...	...	...
		...	...	...	...		...	...	...	...
0.5503	0.280	0.0880	...	...	0.0880		...	...	...	...
		0.0759	...	...	0.0759		...	...	...	...
0.5903	0.320	0.284	...	...	0.284		...	...	...	...
		0.223	...	...	0.223		...	...	...	...
0.6303	0.360	0.578	...	...	0.578		...	...	...	...
		0.429	...	...	0.429		...	...	...	...
0.6703	0.40	0.930	...	...	0.930		...	...	...	...
		0.661	...	...	0.661		...	...	...	...
0.7503	0.480	1.664	0.001	...	1.665		...	...	...	...
		1.150	0.001	...	1.151		...	...	...	...
0.8284	0.558	2.403	0.015	...	2.418	0.0419	0.003	0.006	...	0.009
		1.597	0.014	...	1.611		0.003	0.007	...	0.010
0.8675		...	...	...	...	0.081	0.0063	0.0156	...	0.0219
		...	...	...	...		...	...	...	...
0.9065	0.636	2.972	0.148	...	3.120	0.120	0.039	0.127	...	0.166
		1.949	0.107	...	2.056		0.033	0.109	...	0.142
0.9203	0.650	3.071	0.173	...	3.244	0.134	0.066	0.216	...	0.282
		2.009	0.123	...	2.132		0.054	0.180	...	0.234
0.9865	0.716	3.549	0.270	...	3.819	0.200	0.318	1.068	...	1.386
		2.300	0.180	...	2.480		0.237	0.815	...	1.052
1.0865	0.816	4.185	0.457	...	4.642	0.300	0.797	2.819	...	3.616
		2.642	0.285	...	2.926		0.525	1.972	...	2.497
1.2665	0.996	4.621	0.831	0.108	5.560	0.480	1.146	4.710	0.384	6.240
		3.083	0.541	0.074	3.698		0.767	3.168	0.268	4.203

[a] *l*-av IOSA results.
[b] *l*-in IOSA results.

the low temperature region where the Mitchell and Leroy results[24] deviate significantly. However, we also note that the discrepancy between the two experiments in this temperature range is comparable to that between Mitchell and LeRoy's experiment and theory. We also note that in the case of $v_i = 0$, the experimental and *l*-av IOSA results agree best at the higher temperatures. These contain more contributions from the higher energy collisions for which we believe the IOSA is most accurate.

The results from various theoretical treatments and experiment are compared in Table III. Besides the QCT results [which are also shown in Figs. 15(a) and 15(b)], we also give Garrett and Truhlar's CVT/MCPVAG transition state theory results,[9] Sun *et al.* DWBA results,[8(d)] for $v_i = 0$, and Walker and Hayes' BCRLM results[12] for $v_i = 1$. For $v_i = 0$ the CVT/MCPVAG results are below the IOSA rate constants for the low temperature region, but the higher temperature results from the two methods are reasonably close. The ratio of the IOSA and CVT/MCPVAG is given as a function of temperature in Table IV. The DWBA rate constants are consistently below all the other theoretical rate constants, but the differences decrease as the temperature increases.

For $v_i = 1$, the BCRLM rate constants overlap the IOSA numbers very nicely in the low temperature region, but the deviations become larger as the temperature increases. This is a result of the unnaturally large cross section this model yields once the energy is above the tunneling region.

For $v_i = 1$ there is one experimental result at $T = 300$ K,[25] i.e., $k = 5.9 \times 10^{11}$ cm^3 mol^{-1} s^{-1}. This result is about three times larger than the IOSA rate constant at that temperature.

IV. DISCUSSION

In this work our results derived within the IOSA are compared with all available results obtained by other methods. The QCT,[27] DWBA,[8(d),8(e)] BCRLM,[12] CL-AD-IOSA,[11] and the CVT/MCPVAG.[9] Out of five methods, the first three are capable of supplying numerical answers for any situation. The other two were devised to treat restricted cases only.

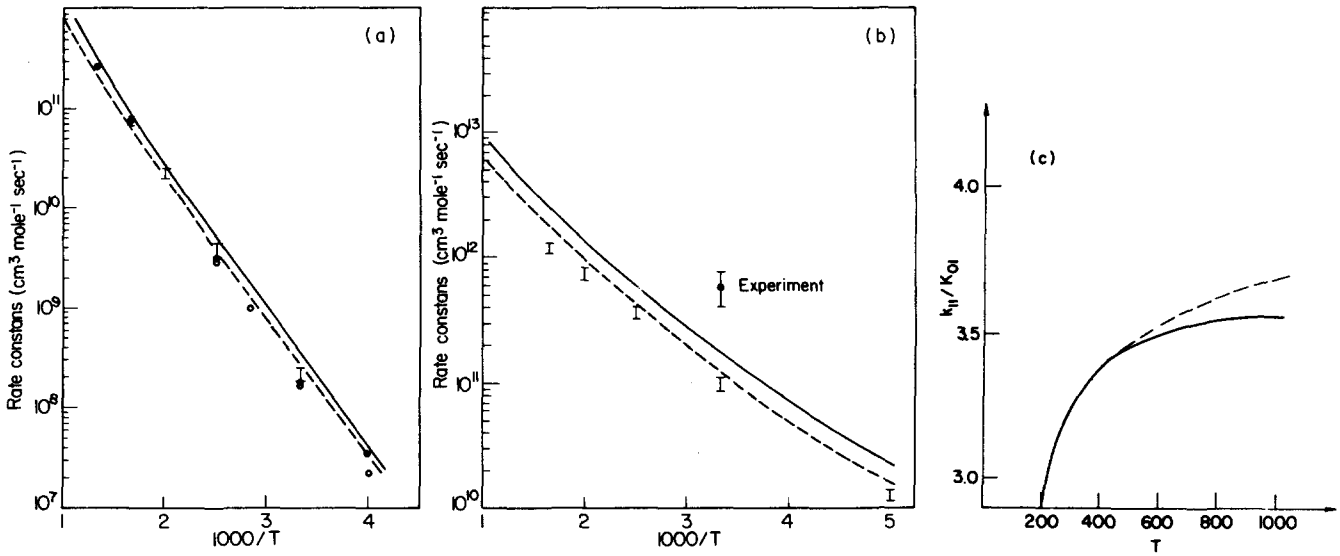

FIG. 16. Total rate constants as a function of temperature. (a) $v_i = 0$; — *l*-av results; --- *l*-in results; | QCT results (Ref. 32); experimental results ● Ref. 23; ○ Ref. 24; (b) $v_i = 1$; — *l*-av results; --- *l*-in results; | QCT results (Ref. 27); ♦ experimental results (Ref. 25); (c) branching ratio — *l*-av; --- *l*-in.

The QCT approach is believed to be reasonably good as long as the energy is not too low (tunneling) and as long as the required result is not too detailed. Thus, total integral and differential cross sections are expected to be reasonably reliable.[6] Moreover, if the tunneling process is not significant then total rate constants should also be reasonably good. From the little known on exact QM results, the QCT is also relevant with respect to rotational distributions.[6] However, QCT seems to perform rather poorly with respect to vibrational state-to-state differential

TABLE II. Vibrational state-to-state and total IOSA rate constants (cm^3 mol^{-1} s^{-1}). Numbers in parentheses are in powers of ten.

T (K)	$v_i = 0$			$v_i = 1$		
	$k_{0\to0}$	$k_{0\to1}$	$k_{0\,\mathrm{tot}}$	$k_{17\to0}$	$k_{l\to1}$	$k_{l\,\mathrm{tot}}$
200	2.15 (6)[a]	...	2.15 (6)	5.68 (9)	1.67 (10)	2.24 (10)
	1.85 (6)[b]	...	1.85 (6)	3.78 (9)	1.10 (10)	1.47 (10)
250	4.31 (7)	8.15 (1)	4.31 (7)	1.75 (10)	5.44 (10)	7.19 (10)
	...	...	...	...	...	...
300	3.35 (8)	4.58 (3)	3.35 (8)	4.10 (10)	1.33 (11)	1.73 (11)
	2.72 (8)	2.97 (3)	2.72 (8)	2.90 (10)	9.40 (10)	1.23 (11)
333.3	9.59 (8)	3.54 (4)	9.59 (8)	6.53 (10)	2.15 (11)	2.70 (11)
	...	...	...	...	...	...
400	4.86 (9)	8.08 (5)	4.86 (9)	1.37 (11)	4.64 (11)	6.02 (11)
	3.82 (9)	4.97 (5)	3.82 (9)	9.79 (10)	3.31 (11)	4.29 (11)
500	2.64 (10)	1.98 (7)	2.64 (10)	3.12 (11)	1.08 (12)	1.39 (12)
	2.02 (10)	1.23 (7)	2.02 (10)	2.20 (11)	7.64 (11)	9.84 (11)
600	8.61 (10)	1.76 (8)	8.63 (10)	5.62 (11)	1.97 (12)	2.53 (12)
	6.43 (10)	1.10 (8)	6.44 (10)	3.93 (11)	1.39 (12)	1.78 (12)
700	2.07 (11)	8.58 (8)	2.08 (11)	8.73 (11)	3.08 (12)	3.95 (12)
	1.52 (11)	5.39 (8)	1.52 (11)	6.04 (11)	2.17 (12)	2.77 (12)
800	4.09 (11)	2.86 (9)	4.12 (11)	1.22 (12)	4.34 (12)	5.56 (12)
	2.95 (11)	1.81 (9)	2.97 (11)	8.41 (11)	3.05 (12)	3.90 (12)
900	7.05 (11)	7.33 (9)	7.12 (11)	1.59 (12)	5.67 (12)	7.26 (12)
	5.02 (11)	4.66 (9)	5.07 (11)	1.09 (12)	3.98 (12)	5.08 (12)
	1.10 (12)	1.57 (10)	1.12 (12)	1.96 (12)	7.00 (12)	8.96 (12)
	7.77 (11)	9.98 (9)	7.87 (11)	1.33 (12)	4.92 (12)	6.27 (12)

[a] *l*-av IOSA results.
[b] *l*-in IOSA results.

TABLE III. Comparisons between the IOSA rate constants and those obtained from other treatments and experiment (cm^3 mol^{-1} s^{-1}). Numbers in parentheses are in powers of ten.

	$v_i = 0$					$v_i = 1$			
T (K)	IOSA[a]	CVT/MCPVAG[b]	DWBA[c]	CL[d]	EXP[e]	IOSA[a]	BCRLM[f]	CL[c]	EXP[g]
200	2.15 (6)	7.41 (5)	2.87 (5)	8.66 (5)	9.09 (5)[h]	2.24 (10)	1.2 (10)	1.29 (10)	...
250	4.31 (7)	1.63 (7)	5.68 (6)	...	3.60 (7)	...	...	...	...
300	3.35 (8)	1.31 (8)	5.43 (7)	2.16 (8)	1.75 (8)	1.73 (11)	1.68 (11)	1.01 (11)	5.9 (11)
400	4.86 (9)	2.47 (9)	1.37 (9)	3.75 (9)	3.06 (9)	6.02 (11)	8.42 (11)	3.61 (11)	...
500	2.64 (10)	...	1.18 (10)	2.22 (10)	...	1.39 (12)	2.41 (12)	7.19 (11)	...
600	8.63 (10)	5.89 (10)	5.37 (10)	8.00 (10)	7.46 (10)	2.53 (12)	...	1.16 (12)	...
1000	1.12 (12)	1.01 (12)	...	...	...	...	...	...	...

[a] *l*-av IOSA.
[b] Reference 9.
[c] Reference 8d.
[d] Reference 32.
[e] Reference 23.
[f] Reference 12.
[g] Reference 25.
[h] Reference 24.

and integral cross sections.[4,5,7] This was shown to be the case on various occasions and *ad hoc* solutions were suggested to improve the results.[7,28]

The DWBA was applied many times to reactive collisions.[8] It seems to yield quite good results for relative rotational and angular distributions. However, it was shown to encounter difficulties whenever total or vibrational state-to-state cross sections were required.[8(e)]

The BCRLM[12] was also derived for treating a general three-dimensional system, but so far only a limited number of results have been published. This method is similar in spirit to the IOSA in the sense that it is based on an exact collinear-like quantum mechanical treatment adjusted to account in the asymptotic region for the appropriate boundary conditions. However, whereas within the IOSA the various noncollinear arrangements are treated explicitly, the BCRLM avoids these treatments by assuming the existence of a quantized bend eigenstate. In this way, for instance, the collinear thresholds for the H(D) + H_2 (v_i = 1) reactions were found to be shifted to a higher energy which yields rather good low temperature rate constants. The physical basis for quantizing the bend in this model is not clear to us because the time taken in traversing the region of intimate interaction is not long compared to the characteristic time to execute the bending motion.[29] Moreover, the BCRLM results seem to us to be much too large at energies somewhat above threshold. For example, for H_2 (v_i = 0, 1) + H and for E_{trans} ~0.7 eV this model yields cross sections which are about four times larger than the QCT total integral cross sections. We do not think the QCT total integral cross sections are likely to differ that much from exact quantum results.

The total integral IOSA cross sections fit the QCT and the AD-IOSA cross sections very nicely, but deviate significantly from those of the DWBA. With respect to rate constants, a somewhat strange situation is encountered because all the published numbers are reasonably close to each other. However, if the experimental results are assumed to be the correct values, then, for v_i = 0, the CVT/MCPVAG, QCT, and IOSA are of a similar quality, whereas the DWBA are somewhat too small for the lower temperature range. For v_i = 1, there is only one experimental value, namely for T = 300 K, and of the three available results, the IOSA and the BCRLM are the closest, although they are still about 300% away.

Not much has appeared in print regarding differential cross sections. The only angular distributions known to us are the QCT[27] and the DWBA[8(a)] for v_i = 0 and E_{trans} = 0.48 eV. Here the QCT results are between the higher IOSA and the lower DWBA results.

Besides the present IOSA results, the only available results for vibrational state-to-state distributions are those due to the DWBA. According to both treatments, the adiabatic 1 → 1 channel is preferred by far over the nonadiabatic channel, but the ratio is three to four within the IOSA vs four to ten within the DWBA. There are strong indications (theoretical and experimental) that the adiabatic channel is really preferred, but is seems to us that the DWBA ratio in the intermediate energy region (~10) is exaggerated.

TABLE IV. Ratio of IOSA to CVT/MCPVAG rate constants as a function of temperature.

T (K)	R
200	2.90
250	2.64
300	2.56
400	1.97
600	1.46
1000	1.11

[1] *The Theory of Chemical Reaction Dynamics,* edited by M. Baer (Chemical Rubber Company, Boca Raton, 1984).
[2] G. C. Schatz and A. Kuppermann, J. Chem. Phys. **62,** 2502 (1975); A. B. Elkowitz and R. E. Wyatt, *ibid.* **62,** 2504 (1975); R. B. Walker, E. B. Stechel, and J. C. Light, *ibid.* **69,** 2922 (1978).
[3] M. Karplus, R. N. Porter, and R. D. Sharma, J. Chem. Phys. **43,** 3259 (1965).
[4] M. Baer, H. R. Mayne, V. Khare, and D. J. Kouri, Chem. Phys. Lett. **72,** 269 (1980).
[5] G. C. Schatz, Chem. Phys. Lett. **94,** 183 (1983); J. Chem. Phys. **79,** 5386 (1983).
[6] G.C. Schatz and A. Kupperman, J. Chem. Phys. **65,** 4668 (1976).
[7] S. Ron, M. Baer, and E. Pollak, J. Chem. Phys. **75,** 4414 (1983).

[8] (a) K. T. Tang, in *Theory of Chemical Reaction Dynamics,* edited by M. Baer (Chemical Rubber Company, Boca Raton, 1984); (b) D. A. Micha, Ark. Fys. **30,** 411, 425, 437 (1965); (c) K. T. Tang and M. Karplus, Phys. Rev. A **4,** 1844 (1971); (d) Y. Y. Yung, B. H. Choi, and K. T. Tang, J. Chem. Phys. **72,** 621 (1980); J. C. Sun, B. H. Choi, R. T. Poe, and K. T. Tang, *ibid.* **73,** 6095 (1980); (e) D. C. Clary and J. N. L. Connor, Mol. Phys. **43,** 621 (1981); (f) C. Zuhrt, F. Schnider, and L. Zulicke, Chem. Phys. **43,** 571 (1976); (g) L. M. Hubbard, S.-H. Shi, and W. H. Miller, J. Chem. Phys. **78,** 2381 (1983); (h) R. W. Emmons and S. H. Suck, Phys. Rev. A **25,** 178 (1982).

[9] B. C. Garrett and D. G. Truhlar, J. Chem. Phys. **72,** 3460 (1980).

[10] R. A. Marcus and M. E. Coltrin, J. Chem. Phys. **67,** 2609 (1977).

[11] (a) E. Pollak, in *Theory of Chemical Reaction Dynamics,* edited by M. Baer (Chemical Rubber Company, Boca Raton, 1984); (b) E. Pollak and R. E. Wyatt, J. Chem. Phys. **78,** 4464 (1983); **81,** 1801 (1984).

[12] R. E. Walker and E. F. Hayes, J. Phys. Chem. **87,** 1255 (1983).

[13] (a) M. Baer, Adv. Chem. Phys. **49,** 191 (1982); (b) J. Jellinek and D. J. Kouri, in *Theory of Chemical Reaction Dynamics,* edited by M. Baer (Chemical Rubber Company, Boca Raton, 1984); (c) V. Khare, D. J. Kouri, and M. Baer, J. Chem. Phys. **71,** 1188 (1979); (d) M. Baer, D. J. Kouri, and J. Jellinek, *ibid.* **80,** 1431 (1984).

[14] (a) D. J. Kouri, V. Khare, and M. Baer, J. Chem. Phys. **75,** 1179 (1981); (b) J. M. Bowman and K. T. Lee, *ibid.* **72,** 507 (1980).

[15] (a) M. Baer, J. Jellinek, and D. J. Kouri, J. Chem. Phys. **78,** 2962 (1983); (b) J. Jellinek, D. J. Kouri, and M. Baer, Phys. Rev. Lett. **47,** 1588 (1981).

[16] N. AbuSalbi, C. L. Shoemaker, D. J. Kouri, J. Jellinek, and M. Baer, J. Chem. Phys. **80,** 3210 (1984).

[17] D. C. Clary and G. Drolshagen, J. Chem. Phys. **76,** 5027 (1982).

[18] D. C. Clary, Chem. Phys. **81,** 379 (1983).

[19] N. AbuSalbi, D. J. Kouri, Y. Shima, and M. Baer, Chem. Phys. Lett. **105,** 472 (1984).

[20] M. J. Redmon and R. E. Wyatt, Chem. Phys. Lett. **63,** 209 (1979); R. E. Wyatt, J. F. McNutt, and M. J. Redmon, Ber. Bunsenges. Phys. Chem. **86,** 437 (1982); R. E. Wyatt and M. J. Redmon, Chem. Phys. Lett. **96,** 284 (1983).

[21] S. Ron, E. Pollak, and M. Baer, J. Chem. Phys. **79,** 5204 (1983).

[22] P. Siegbahn and B. Liu, J. Chem. Phys. **68,** 2457 (1978); D. G. Truhlar and C. J. Horowitz, *ibid.* **68,** 2466 (1978); **71,** 1514 (1979).

[23] A. A. Westenberg and N. De Haas, J. Chem. Phys. **47,** 1393 (1967).

[24] D. N. Mitchell and D. J. LeRoy, J. Chem. Phys. **58,** 3449 (1973).

[25] G. P. Glass and B. K. Chatuverdi, J. Chem. Phys. **77,** 3478 (1982).

[26] J. Geddes, H. F. Krause, and W. L. Fite, J. Chem. Phys. **56,** 3298 (1972).

[27] H. R. Mayne and J. P. Toennies, J. Chem. Phys. **75,** 1794 (1981).

[28] C. J. Ashton, J. T. Muckerman, and F.E. Schubert, J. Chem. Phys. (in press).

[29] N. AbuSalbi, M. Baer, D. J. Kouri, and E. Pollak (submitted for publication).